NJC

PAPER

View Article Online
View Journal

Cite this: DOI: 10.1039/c7nj01828b

Versatile coordination ability of thioamide ligand in Ru(II) complexes: synthesis, computational studies, *in vitro* anticancer activity and apoptosis induction†

Ramasamy Raj Kumar, [a] Rengan Ramesh *[a] and Jan Grzegorz Małecki [b]

The reaction of a (2-hydroxy-5-nitrophenyl)(pyrrolidin-1-yl) methanethione ligand (**L**), with an equimolar amount of [RuHCl(CO)(PPh_3)$_3$] afforded two structurally different ruthenium(II) complexes of formulas [Ru(CO)(Cl)(PPh_3)$_2$(O^S)] (**1**) and [Ru(CO)(PPh_3)$_2$(N^O^S)] (**2**) by varying the experimental reactions conditions. Interestingly, the ligand behaves in a monobasic bidendate OS fashion in reflux conditions *vis* C–N bond cleavage, while it acts as a dibasic tridendate NOS donor at room temperature towards the ruthenium(II) precursor. The synthesised ruthenium complexes **1** and **2** are fully characterized by means of analytical (elemental analysis), spectral [FT-IR, UV-vis, NMR (^{1}H, ^{13}C and ^{31}P)] and fluorescence methods, respectively. The solid state molecular structures of the ligand and the complexes were studied by using single crystal X-ray crystallography, which confirms the different coordination mode of the ligand with the ruthenium ion and reveals the presence of distorted octahedral geometry. Notably, in complex **1**, the two triphenylphosphine co-ligands occupy trans positions, whereas in complex **2** they are mutually cis disposed. The intercontacts in the crystal structures are examined using Hirshfeld surface analysis. The stability of the complexes is also studied by time-dependent UV-visible and ESI-mass spectral methods. Moreover, the cytotoxic effect of the complexes is examined on cancerous cell lines such as HeLa and MCF-7 along with a cell viability assay against non-cancerous NIH-3T3 cells under *in vitro* conditions and the results showed that the complexes exhibit significant anticancer activity. Furthermore, the morphological changes and apoptosis induction have been studied by AO-EB dual staining methods, Hoechst 33258 and flow cytometry techniques.

Received 25th May 2017,
Accepted 20th July 2017

DOI: 10.1039/c7nj01828b

rsc.li/njc

Introduction

In recent years, there has been a surge in the development of thioamide-based ligands designed for biologically active transition metal complexes. Thioamides are sulphur analogues of amides and are a starting material for the preparation of thiazoles, amidenes and amidrazones which coordinate strongly with metal ions. The chemical interest arises from the ability of thioamides to adopt various coordination modes, leading to enormous structural diversity of their metal complexes. They can easily be modified by variation of the parent aldehydes or ketone for synthesis. These ligands are vital structural motifs widely used as key intermediates and versatile building blocks for the construction of biologically important sulphur-containing heterocycles.[1,2] They are of considerable pharmacological interest since a number of derivatives have shown a broad spectrum of chemotherapeutic properties. In particular, heterocyclic thioamides have antibacterial, antineoplastic, antimalarial, antiviral and antitumour activities.[3–5] Although uncomplexed thioamides show interesting biological activity, metal complexes of thioamides show a marked increase in activity.[6,7] Currently, considerable effort is being directed towards the synthesis and structural characterization of metal complexes of aromatic thioamides,[8–11] due to their highly interesting chemical and biological properties.[12,13]

The amide bond is a crucial backbone in organic chemistry and constitutes the key functional group in peptides, polymers, and many natural products and pharmaceuticals.[14] The significant increase in the interest in the reactivity of transition metals leading to the cleavage of C–X bonds (where X = O, S, N)[15] can be attributed to how this nature can lead to new chemical

[a] *Centre for Organometallic Chemistry, School of Chemistry, Bharathidasan University, Tiruchirappalli-620 024, Tamil Nadu, India. E-mail: ramesh_bdu@yahoo.com, rramesh@bdu.ac.in; Fax: +91-431-2407045, +91-431-2407020; Tel: +91-431-2407053*

[b] *Department of Crystallography, Institute of Chemistry, University of Silesia, 40-006 Katowice, Poland*

† Electronic supplementary information (ESI) available: ^{1}H, ^{13}C and ^{31}P NMR spectra for the ligand and complexes (**1–2**), ESI-Mass, stability studies and MTT assay for the complexes. CCDC 1472340, 1473794 and 1518538. For ESI and crystallographic data in CIF or other electronic format see DOI: 10.1039/c7nj01828b

transformations with practical implications for several industrial processes. Dehydrodesulfurization,[16] deoxygenation,[17] and denitrogenation[18] of crude oil, catalytic degradation of halocarbons,[19] and catalysis and extrusion of nitrogen and ammonia from organic compounds[20] are the most prominent examples among a plethora of reactions which involve C–X bond cleavage. Although some of these processes are well understood, reactions leading to the cleavage of the C–N bonds are particularly challenging and information on them remains scarce.[21] There have been few reports on transition-metal-mediated cleavage of aliphatic C–N bonds.[22–25] Rupture and repair of the porphyrin inner core: carbon–nitrogen bond breaking and formation in ruthenium complexes of an *N*,*N*′-bridged porphyrin have been described.[26] The C–N bond cleavage of anilines by a (Salen)ruthenium(VI) nitrido complex has been reported.[27] Amide C–N bond cleavage and formation of nitride promoted by a niobium(II) cluster has been reported by Tayebani *et al.*[28] Facile C–N cleavage in a series of bridged lactams has been reported.[29] The activation of the relatively inert C–N bonds of anilines under mild conditions has been reported.[30] Catalytic C–C bond formation reactions proceeding *via* cleavage of C–N bonds in aniline derivatives through catalysis by the ruthenium complex $[RuH_2(CO)(PPh_3)_3]$ have also been reported in the literature.[31] Recently, solvent-assisted formation of ruthenium(II)/copper(I) complexes containing thiourea derivatives has been reported from *in vitro* biological perspectives in which the ligand underwent C–N cleavage during complex formation.[32]

Cisplatin and its analogues are still one of the world's best-selling anticancer drugs. The limitation of using cisplatin is that it leads to side effects and dose-limiting nephrotoxicity and the development of drug resistance prevents its potential efficacy.[33] Nevertheless, this limited effectiveness due to severe side effects and acquired resistance due to prolonged treatment has spurred investigators to find alternative metal-based drugs. Among the different metal complexes generating interest, ruthenium complexes have shown great potential and remain the subject of extensive drug discovery efforts.[34,35] In this respect, ruthenium complexes are better suited because of their variable oxidation states, low toxicity, selectivity for cancer cells, ability to penetrate tumor cells reasonably well, ability to bind effectively to DNA and ability to mimic iron in binding to biomolecules.[36]

To the best of our knowledge, reports on thioamide ligands undergoing amide C–N bond cleavage are scarce in the literature. Therefore, in this investigation, we have taken a ruthenium unit along with a (2-hydroxy-5-nitrophenyl)(pyrrolidin-1-yl) methanethione ligand. In an effort to substantiate this speculation, the chemistry of structurally diverse ruthenium(II) complexes is described in this paper along with synthesis, crystal structures and *in vitro* anticancer activities. To get an insight into the geometry and the electronic structure of these complexes, density functional theory (DFT) studies have also been included. Based on X-ray diffraction, Hirshfeld surface analysis and the 2D Finger plots have been analysed and visualized. In addition, the *in vitro* anticancer activity of the complexes against human cancer cell lines by MTT assay and the mechanism of cell death were investigated using AO-EB, Hoechst 33258 staining methods and flow cytometry analysis.

Results and discussion

Synthesis of the complexes

Reaction of the (2-hydroxy-5-nitrophenyl)(pyrrolidin-1-yl) methanethione ligand (**L**) with an equimolar amount of $[RuHCl(CO)(PPh_3)_3]$ resulted in two different entities, namely $[Ru(CO)(Cl)(PPh_3)_2(O\text{^}S)]$ (**1**) and $[Ru(CO)(PPh_3)_2(N\text{^}O\text{^}S)]$ (**2**), with different structural features by varying the reaction conditions. The ligand behaves as a monobasic bidendate (O, S) which undergoes C–N bond cleavage resulting in the formation of a new ruthenium(II) benzothialdehyde complex (**1**) in benzene medium under reflux conditions. However, the same ligand acts as a dibasic tridendate (OSN) in complex (**2**) under stirring in benzene at room temperature. Coordination was immediate, as a change of colour from yellow to red was observed. Both the ruthenium(II) complexes have been isolated as red coloured, air stable solids and are non-hygroscopic in nature. The complexes were isolated as red solid in 72–80% yield (Scheme 1). The new ruthenium complexes are highly soluble in polar organic solvents such as chloroform, dichloromethane, acetonitrile, DMF and DMSO. They are found to be diamagnetic, characteristic of the low-spin d^6 ruthenium(II) complexes. The identities of the complexes were confirmed by using elemental analysis, NMR, mass and X-ray analysis. The analytical data of the two ruthenium complexes are in good agreement with the molecular formula proposed.

We take into account that when the starting precursor is a ruthenium hydride complex $[RuH(Cl)(CO)(PPh_3)_3]$, the acid–base reaction conditions have an impact on the reaction products. At boiling temperature, the strongly stressed coordinated ligand is vulnerable to nucleophilic attack and the C–N bond is broken. Moreover, the negative potential in the studied complex wraps the sulphur and nitrogen atoms (*cf.* Fig. S1 in the ESI†) and the potentials on the halogen atoms are considerably lower than the ones on the S or N atoms. This shows that the C–N bond in the coordinated ligand is susceptible to substitution. The C═S bond distance in the free ligand and in complex **1** is 1.67 and 1.63 Å respectively, whereas the C–S bond distance in complex **2** is 1.83 Å, indicating a partial double bond character in C═S bonds and a weakening of the C–S bond after coordination by the ligand to the metal centre.

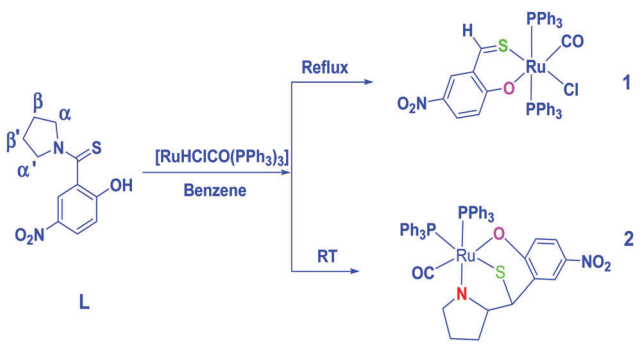

Scheme 1 Synthetic route for the ruthenium(II) complexes **1** and **2**. The coordinating atoms are shown in distinct colours.

Spectroscopic characterization of the complexes

FT-IR spectra. The IR spectrum of the free ligand displayed characteristic stretching bands at 3172 and 765 cm^{-1} due to its –OH and C=S functional groups.[37] The –OH stretching vibrations are not observed in the complexes, which indicates that the ligand underwent tautomerization and subsequent coordination to ruthenium metal *via* the phenolic oxygen upon complexation. The band observed in the region of 1315–1316 cm^{-1} due to (ν_{C-O}) further confirms the coordination through the phenolic oxygen.[38] A strong band in the region of 1953 to 1954 cm^{-1} is due to the terminally coordinated carbonyl group and is observed at a slightly higher frequency than in the precursor ruthenium complexes. In addition, a set of four bands at 540, 695, 745 and 1434 cm^{-1} in the spectra of the complexes was attributed to ruthenium bound triphenylphosphine groups.[39] A band is observed at 744 cm^{-1} in complex **1** which corresponds to the coordination of thione sulphur to the ruthenium(II) ion and a Ru–Cl stretching mode appears in the region of 425 cm^{-1} respectively.[40] Moreover, complex **2** displays new bands at 695 cm^{-1} and 518 cm^{-1} corresponding to ν_{C-S} (thiol sulphur) and ν_{Ru-N} stretching modes respectively. The coordination of thiol sulphur to ruthenium is further supported by the lengthening of the C–S bond, which is evidenced by the X-ray structure. Based on the IR spectral data it is clearly inferred that the ligand is coordinated to the ruthenium(II) ion in a bidendate mode *via* the phenolic oxygen and thione sulphur in complex **1** whereas the ligand binds to ruthenium(II) ion in a tridentate mode through the pyrrolidine nitrogen, phenolic oxygen and thiolate sulphur in complex **2**. The experimental and calculated infrared spectra of the complexes in KBr pellets are given in Fig. S2 (ESI†).

Electronic spectra. The electronic absorption spectra of the complexes in dry $CHCl_3$ showed three to four bands in the region of 240–600 nm. The ground state of ruthenium(II) in an octahedral environment is $^1A_{1g}$, arising from the t_{2g}^6 configuration, and the excited states corresponding to the $t_{2g}^5 e_g^1$ configurations are $^3T_{1g}$, $^3T_{2g}$, $^1T_{1g}$, and $^1T_{2g}$. Hence, four bands corresponding to the $^1A_{1g} \rightarrow {}^3T_{1g}$, $^1A_{1g} \rightarrow {}^3T_{2g}$, $^1A_{1g} \rightarrow {}^1T_{1g}$ and $^1A_{1g} \rightarrow {}^1T_{2g}$ transitions are possible in order of increasing energy. The bands around 600–555 nm and 395–414 nm are assigned to $^1A_{1g} \rightarrow {}^1T_{1g}$ and charge transfer transitions respectively. The charge transfer bands observed in the complexes due to M → L transition are possible in the visible region. Moreover, the presence of carbonyl, triphenylphosphine and heterocyclic bases as ligands, which are capable of producing a strong ligand field increasing e_g^* orbital, places these levels relatively high in energy. Therefore, the lowest charge transfer bands due to excitation of an electron from the metal t_{2g} level to an unfilled molecular orbital derived from the π* ligands level should appear in a relatively higher energy region compared to those due to $t_{2g} \rightarrow e_g^*$ transitions.[41,42] The high intensity bands in the region of 240–270 nm were characterized by the ligand-centered transitions and have been designated as π–π* and n–π* transitions for the electrons localized on the thioamide ligand. The pattern of the electronic spectra of the complexes indicated the presence of an octahedral environment around the ruthenium(II) ion, similar to other formerly reported ruthenium(II) complexes.[41]

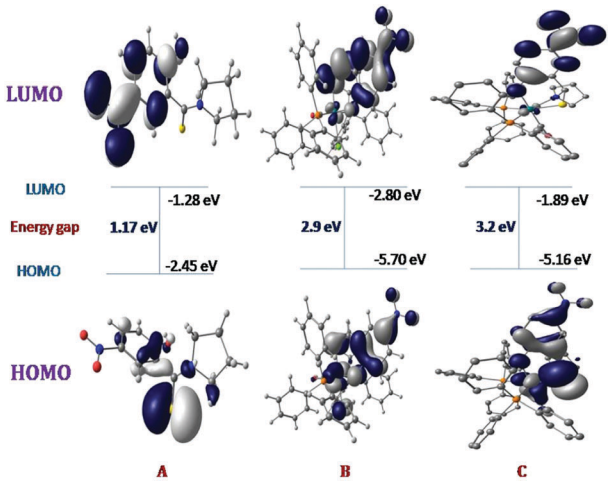

Fig. 1 Frontier molecular orbitals of the ligand (**A**) and complexes (**B–C**), and their energy gaps.

To get an insight into the electronic structures of the ruthenium complexes, calculations with the DFT method at the B3LYP/6-31G**/DZVP (the DZVP basis was used for the ruthenium(II) ion) level were carried out. Contour plots of the molecular orbitals of the ligand and complexes were generated using Gauss view 9.0 and the frontier molecular orbitals of A–C were determined and are depicted in Fig. 1. Moreover, analysis of the frontier molecular orbitals is useful for understanding the spectroscopic properties such as electronic absorption and emission spectra. So, the density of states (DOS) and overlap population density of states (OPDOS) in terms of Müllikan population analysis were calculated and the pictorial representation of the MO compositions and their contributions to the chemical bonding are presented in Fig. S3 and S4 (ESI†). Based on the calculated electronic structures of the complexes, the absorption spectra of the complexes **1** and **2**, and the lowest energy, broad and low intensity absorption bands on the UV-vis spectra, the complexes have a metal-to-ligand charge transfer character.

Further, the composition of the frontier HOMOs and LUMO/L+1 indicates that the MLCT transitions are accompanied by charge transfer from the chloride to L and intraligand transitions. A similar character is indicated by the second absorption band with a maximum at 395 nm but in this band the charge transfer between triphenylphosphine and **L** plays a crucial role because the transitions between lower occupied molecular orbitals and the LUMO were calculated in the energy range. The higher energy bands are attributed to transitions of ligand–ligand charge transfer type. The results of the experimental absorption measurements resemble the theoretically calculated results. The experimental and calculated UV-vis spectra of complexes **1** and **2** with the calculated electronic transitions are shown in Fig. S5 (ESI†).

NMR spectra. Evidence of chelation can also be obtained from the NMR spectra of the ligand and the ruthenium complexes. The ^1H NMR spectra of the free ligand and complexes were recorded in $CDCl_3$ solution and the spectra are depicted in Fig. S6 and S8 (ESI†). In the ^1H NMR spectra, the signal due to the phenolic –OH

and four methylene groups (pyrrolidine ring) of the free ligand (**L**) appear at 9.8 and 2.0–3.9 ppm, respectively. The –OH groups are absent in the spectra of the complexes, supporting the deprotonation and coordination *via* the phenolic oxygen to the ruthenium(II) ion. This fact confirms the deprotonation of the ligand which is also confirmed by the IR data. In the NMR spectrum of the free ligand, four methylene groups (pyrrolidine ring) on the thioamide-N atoms appeared separately, suggesting their non-equivalence and slow-rotation of the thioamide C–N bond on the NMR time scale.[43,44] In complex **1**, the (–HC═S) proton appears as a singlet in the region of 8.0 ppm; also, methylene groups in the pyrrolidine ring signal disappear in the aliphatic region of 2.0–3.9 ppm suggesting the cleavage of the amide C–N bond. The overlapping multiplets observed in the region around δ 7.1–7.6 ppm are due to the presence of aromatic protons and triphenylphosphine groups. Interestingly, the methylene protons of the pyrrolidine ring are observed in the region of 2.7–3.8 ppm suggesting that the pyrolidine ring is involved in coordination *via* nitrogen to the ruthenium ion in complex **2**. The ^{13}C NMR spectra of the ligand and ruthenium complexes were recorded in $CDCl_3$ solutions and the spectra are shown in Fig. S7 and S9 (ESI†). The ^{13}C NMR spectra clearly showed that the chemical shift of the thioketone carbon moves upfield from 189 ppm in the ligand to 158–170 ppm in the ruthenium complexes, indicating the reduced C–S bond order upon complexation. The aromatic carbons of the free ligand and triphenylphosphines in the complexes show signals in the region of 117–140 ppm. The ^{13}C NMR spectra of the complexes showed peaks at 186 and 190 ppm corresponding to the terminal carbonyl group. The methylene and methine carbons in complex **2** show signals at 24–53 ppm. The coordination of the triphenylphosphines as co-ligands and their configuration in the ruthenium complexes **1–2** are confirmed from the ^{31}P NMR of single crystals of the ruthenium complexes and the spectra are shown in Fig. S10 (ESI†). The appearance of a singlet at δ 27.2 and 43.3 ppm for complex **1** and **2** suggests the presence of two magnetically equivalent triphenylphosphines. The NMR spectra of the complexes **1** and **2** therefore confirm the coordination mode of the ligand to the Ru(II) ion and the results are consistent with the molecular structures revealed by X-ray diffraction studies.

X-ray crystallographic studies. As part of the structural characterization, the molecular structure of the ligand (**L**) and the complexes **1** and **2** have been determined by single crystal X-ray analysis. The single crystals of the ligand and complexes were obtained from the slow evaporation method using methanol and dichloromethane–acetonitrile solvents. Perspective views of the molecular structures with the atom numbering scheme are depicted in Fig. 2–4. The summary of the data collection and refinement parameters are given in Table S1 (ESI†). Whereas selected bond lengths and bond angles are gathered in Table S2 (ESI†).

In complex **1**, the facile cleavage of the C–N bond during reaction of **L** with the ruthenium(II) precursor is unexpected and seems to be metal-induced amide bond cleavage as shown in Scheme 1. [Ru(CO)(Cl)(PPh$_3$)$_2$(O^S)] (**1**) crystallizes in the monoclinic space group $P2_1/n$ and the structure of the complex is shown in Fig. 3. The crystal structure also reveals the

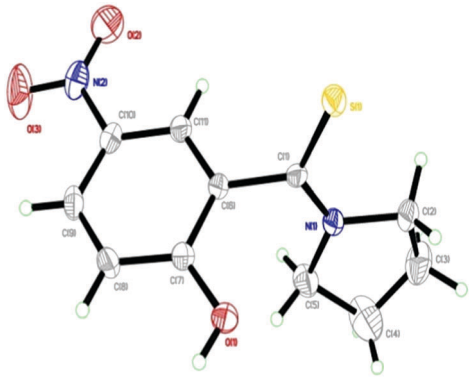

Fig. 2 ORTEP view of the ligand with 30% probability level.

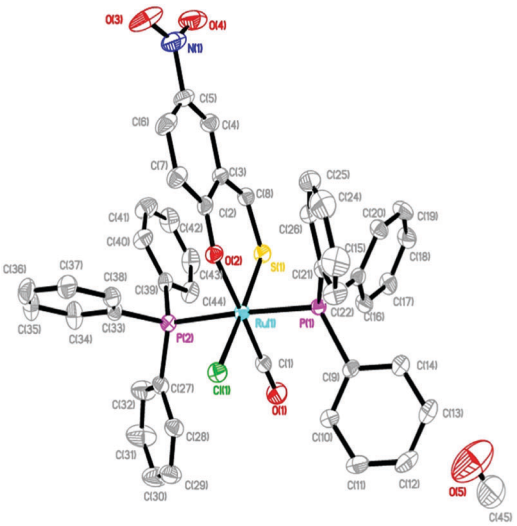

Fig. 3 ORTEP diagram of complex **1** in CH_3OH at the 30% probability level, with hydrogen atoms being omitted for clarity.

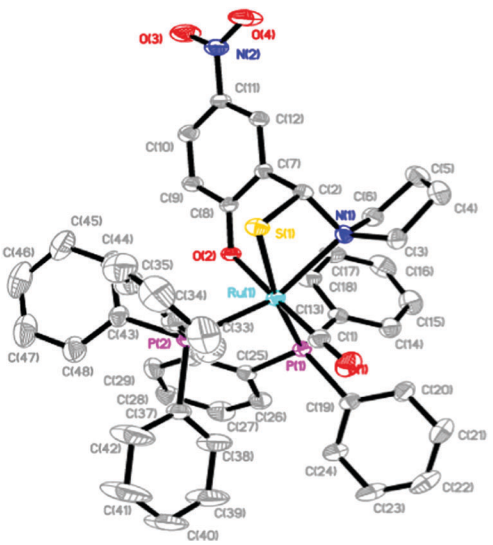

Fig. 4 ORTEP diagram of complex **2** at the 30% probability level, with hydrogen atoms being omitted for clarity.

presence of two solvent molecules (CH_3OH) per complex. The ligand coordinates in a bidendate manner to the Ru(II) *via* the O, S donors forming one six membered chelate ring. One carbonyl group (*trans* to the phenolic oxygen) and one chloride ion form an OSCOCl square plane and the phosphorous atoms of the two triphenylphosphine ligands occupy the two axial sites. However, the presence of a strong π-acidic character of CO in the complex has probably forced the bulky PPh_3 to take up mutually trans positions for steric reasons. Ruthenium is therefore sitting in an $OSCOClP_2$ coordination environment, which is distorted octahedral in nature as reflected in all the bond parameters around ruthenium. The bite angles around the Ru(II) ion, O(2)–Ru(1)–S(1), O(2)–Ru(1)–P(1), and S(1)–Ru(1)–P(1), are equal to 90.62(5)°, 91.77(5)° and 89.93(3)°, respectively, and the bond lengths are 2.2916(7) Å for Ru(1)–S(1), 2.0914(16) Å for Ru(1)–O(2), 2.4133(6) Å for Ru(1)–Cl(1) and 1.637(3) Å for C(8)–S(1). The two triphenylphosphine ligands are mutually trans disposed with Ru(1)–P(1) and Ru(1)–P(2) distances of 2.4045(7) and 2.4268(7) Å, respectively. The two Ru–P bond lengths are similar and comparable with those found in other reported ruthenium complexes containing PPh_3.[45] The Ru(1)–O(2) distance equal to 2.0914(16) Å is shorter than Ru(1)–S(1) 2.2916(7) Å. The thione form is confirmed by the bond length of C(8)–S(1) being 1.637(3) Å, which is very close to a formal C=S bond length (1.676(2) Å). In the complexes, the C=S bond distances are no longer than that of the free ligand but the phenolic C–O bond length is slightly reduced upon coordination of the ligand to the ruthenium. The bond lengths and bond angles are in good agreement with reported data on related ruthenium(II) complexes.[46,47]

In the free ligand, the amide C–N bond distance is equal to 1.310(3) Å, which is elongated up to 1.520(3) Å after coordination to ruthenium(II). Furthermore, the geometry of the thioamide part of the ligand changes significantly during the complexation. The S–C–N angle decreases from 122.56(18)° in the free ligand to 103.03(15)° in the complex **2**. The data indicate a strong weakness of the amide bond (activation). So under mild reaction conditions (room temperature) complex **2** can be isolated.

$[Ru(CO)(PPh_3)_2(N\hat{}O\hat{}S)]$ (**2**) crystallized in the monoclinic space group $P2_1/n$ and the structure of the complex is given in Fig. 4. The thioamide ligand behaves in a tridentate manner and coordinates to the Ru(II) *via* the pyrrolidine nitrogen N, phenolic O and thiolate S donors forming one four and one six membered chelate ring. In addition, one carbonyl group (*trans* to the phenolic oxygen) and pyrrolidine nitrogen also coordinate to the Ru(II) ion to form a NOSCO square plane and the phosphorous atoms of the two triphenylphosphine ligands occupy the *cis* position for better Π interaction.[45] Hence, ruthenium is placed in a $NOSCOP_2$ coordination environment, which is distorted octahedral in nature as reflected in all the bond parameters around ruthenium. This complex displays a significantly distorted octahedral geometry imposed on by its four and six membered chelate rings. The bite angles around the Ru(II) ion are O(2)–Ru(1)–S(1) 88.01(5)°, O(2)–Ru(1)–P(1) 84.60(5)°, O(2)–Ru(1)–P(2) 94.32(5)° and N(1)–Ru(1)–S(1) 68.82(6)° with bond lengths of 2.3976(7) Å for Ru(1)–S(1), 2.1090(16) Å for Ru(1)–O(2) and 1.835(3) Å for C(2)–S(1). The two triphenylphosphine ligands are mutually *cis* disposed with Ru(1)–P(1) and Ru(1)–P(2) distances of 2.4084(7) and 2.3627(7) Å, respectively. The two Ru–P bond lengths are similar and comparable with those found in other reported ruthenium complexes containing PPh_3.[48] In addition, the Ru–N bond length equal to 2.259(2) Å is comparable with other reported ruthenium complexes.[49] The thiol form is confirmed by the bond length of C(2)–S(1) 1.835(3) Å which is very close to other ruthenium complexes. The bond lengths and bond angles are in good agreement with reported data on related octahedral ruthenium(II) complexes.[50]

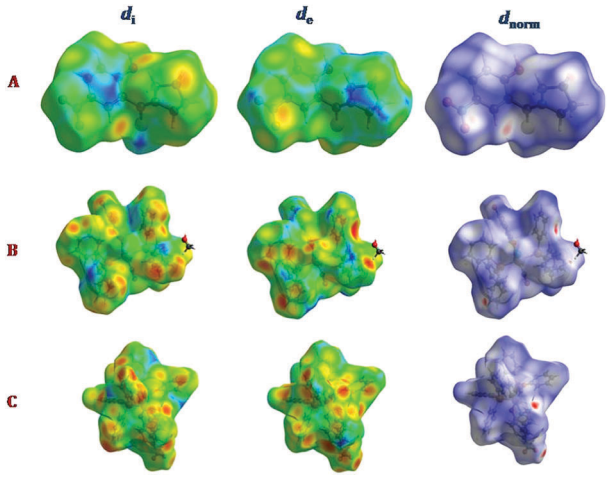

Fig. 5 Hirshfeld surfaces for the ligand (**L**) and complexes **1** and **2** mapped with d_i, d_e, and d_{norm} (A–C).

We analysed the intermolecular interactions in the crystal structures of the free ligand and ruthenium complexes using Hirshfeld surface analysis. This approach is a graphical tool for visualizing and understanding intermolecular interactions.[51] In Fig. 5 are presented the Hirshfeld surfaces on which are mapped the internal distances (d_i), *i.e.* the distances from the surface to the nearest nucleus inside, outside surface (d_e) and normalized contact distance (d_{norm}), defined in terms of d_e, d_i and the vdW radii of the atoms.

The share of each molecular interaction is shown in Fig. 6 and hydrogen bonds for the ligand and complexes are gathered in Table S3 (ESI†). In the structures of **L** and complexes **1** and **2**, a dominant role is played by the H···H interactions with distances around (white colour on the d_{norm} surface) and longer (blue colour) than the van der Waals radii separation. The O···H and H···O contacts, *i.e.* hydrogen bonding, comprise 30.5% of the total Hirshfeld surface area of the **L** molecule. The S···H and *vice versa* interactions, which create the infinite H-bond chain (*cf.* Fig. S11 in (ESI†), participate in the surface area with 14.6% and display the wings on the 2D fingerplot at top left and bottom right. The top wing ($d_i < d_e$) corresponds to the O–H donor, whereas that at the bottom right ($d_e < d_i$) corresponds to the surface around the S acceptor.

The H···H interactions play a major role covering 55% and 59% of the total Hirshfeld surface areas in the case of **1** and **2** respectively. The C···H, *i.e.* C–H···π, interactions are present in

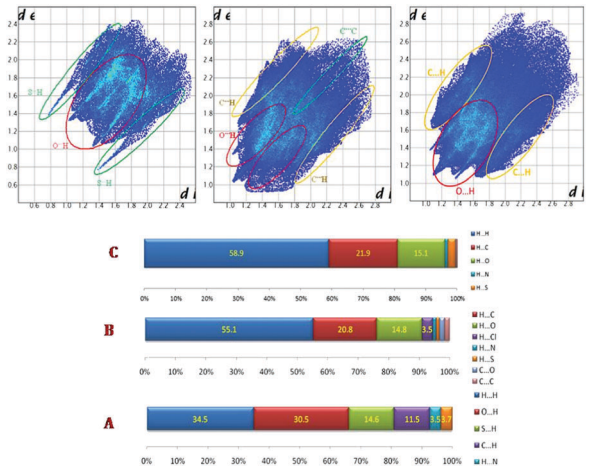

Fig. 6 2D fingerprint plots and percentage contributions to the Hirshfeld surface area for the ligand and complexes **1** and **2**(A–C). Percentages are given on the histogram only for the major atom-type/atom-type contacts.

both ruthenium complexes and participate in the area with about 21% and 22% share, and the C···C that is π···π interaction participates only in the structure of complex **1** in the surface, contributing 1.6%. However, in the same compound, a similar contribution comes from N···O contact (1.7%), which in this case means the N–O···π interaction. The parameters of these intermolecular interactions in the structures of the complexes are summarized in Table S4 (ESI†). The analysis shows that in the case of **1** the π-stacking, N···O/N–O···π and H···Cl interactions affect, to a certain extent, the structural stabilization as compared to complex **2**. The TGA curves show that the complex **1** is stable upto 200 °C and the decomposition of **2** starts at 160 °C as shown in Fig. S12 (ESI†). The lower stability of **2** is connected on one hand with the presence of the pyrrolidine moiety in the ligand which causes stress in the coordinated ligand. On the other hand the mentioned above intermolecular interactions in **1** play a stabilizing role.

Emission properties. The ruthenium(II) complexes containing strong chromophoric groups often show, in addition to intense MLCT transitions, interesting luminescence properties; such properties have also been explored in this type of complex. The luminescence studies of the complexes were carried out in degassed chloroform solution at room temperature and are illustrated in Fig. S13 (ESI†). When an excitation wavelength corresponding to the lowest energy absorption ~400 nm was used, no emission was observed. However, when an excitation wavelength of 560 nm was used, the two ruthenium complexes showed red emission falling within 615–630 nm. It is likely that the emission originates from the lowest energy metal-to-ligand charge transfer (MLCT) state, probably involving dπ(Ru)–π*(ligand) transitions, similar to the MLCT observed in Ru(II) bipyridyl complexes.[52] The complexes are luminescent in nature at room temperature and possess light emitting properties. This assignment is also supported by the analysis of the frontier orbitals of the complexes. The dichloromethane solutions of the compounds excited at 560 nm reveal emission with a maximum at 613 nm. The excitation wavelength corresponds to the H−1 → LUMO

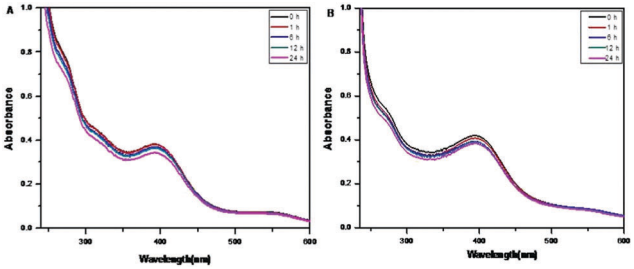

Fig. 7 UV-vis absorption spectrum of complexes **1**(A) and **2**(B) in aqueous PBS buffer solution, at pH 7.4, to a final concentration of 1×10^{-3} M recorded after different time intervals.

(80%) (71%) and HOMO → L+1 (71%), indicating that the transition has MLCT character.

Stability studies. A reasonable stability in aqueous media plays an important role for the development of anticancer drug candidates. The solution chemistry of the complexes **1** and **2** are studied by time-dependent UV-visible absorption spectroscopy. The complexes are first dissolved in DMSO, and the concentrated DMSO solutions were diluted using aqueous PBS buffer, at pH 7.4, to a final concentration of 1×10^{-3} M. The UV-visible absorption spectra of these solutions are recorded for different time intervals over 24 h at room temperature and shown in Fig. 7. In addition, the stability of the complexes in DMSO was also monitored at various time intervals and the spectra are shown in Fig. S14 (ESI†). The spectral profiles for complexes **1** and **2** did not change, which clearly indicates the stability nature of the complexes in DMSO and aqueous medium. These absorption bands remain unchanged over 24 h, and also no new absorption bands were observed during the experimental period showing the substantial stability of the complexes in DMSO and PBS buffer solutions.

Furthermore, information about the composition of the complexes was also acquired from ESI-MS spectral studies. Hence, we have recorded mass spectra for the complexes **1** and **2** and they are shown in Fig. S15 (ESI†). Mass spectrometric measurements were carried out under positive ion ESI conditions with different cone voltages, using acetonitrile as the solvent and the mobile phase. The ESI spectra of complexes **1** and **2** exhibit base peaks at *m*/*z* 871.0 and *m*/*z* 905.2, respectively.

In vitro anticancer activity

Cancer cell growth inhibition (MTT assay). The antiproliferative activities of the ruthenium complexes were measured against HeLa and MCF-7 along with NIH 3T3 cell lines by using the MTT [3-(4,5-dimethylthiazol-2-yl)-2,5-diphenyltetrazoliumbromide] assay (colorimetric assay) and the widely used clinical drug, cisplatin, was included as a positive control. The ability of the ruthenium(II) complexes to arrest the proliferation of cancer cells was investigated after exposure for 48 h. The cytotoxicity results were specified by means of cell viability curves and expressed with values in the studied concentration range from 0.1–100 μM. The activities corresponding to inhibition of cancer cell growth at the maximum level, indicated as IC_{50} values linked to inhibition of cancer cell growth at the 50% level, are noted. It is to be noted that the

Table 1 Cytotoxicity (IC_{50}, μM) of the ligand and complexes **1** and **2** (n. e.: no effect), selectivity index (SI) and calculated partition coefficients (log *P*)

	IC_{50} values (μM)					
Complexes	HeLa	SI	MCF-7	SI	NIH-3T3	log *P*
1	45.6 ± 0.2	5.40	43.6 ± 0.5	5.65	246.60 ± 0.8	−0.82
2	60.7 ± 0.6	4.11	57.3 ± 1.2	4.35	249.48 ± 0.4	−1.23
L	n.e.	—	n.e.	—	n.e.	—
Cisplatin	21.3 ± 0.2	11.38	19.5 ± 0.6	12.43	242.52 ± 0.6	—

precursor and the ligand did not show any inhibition of the cell growth even up to 300 μM which clearly indicates that chelation of the ligand with a metal ion is important for the observed cytotoxicity properties of the complexes.

The resulting 50% growth inhibitory concentration (IC_{50}) values are summarized in Table 1 and graphically depicted in Fig. S16 (ESI†). From the experimental results, the IC_{50} values show that complex **1** (bidendate mode) exhibits a slightly higher inhibitory effect than complex **2** (tridentate) towards the tested cancer cell lines indicating that the leaving group, and as consequence the aquation rate, plays an important role in the anticancer activity. Another factor that has been considered as important in anticancer activity of metal complexes is their hydrophobicity. So, we have investigated the hydrophobicity of the present ruthenium complexes, which can be related to their cytotoxicity. The calculated log *P* values are −0.82 and −1.23 for complex **1** and **2** respectively. Complex **1** has the highest log *P* value and therefore enhances the hydrophobicity to facilitate the crossing of the cell membrane, which of leads to cell death as a possible mechanism. The results of MTT assays revealed that the complexes showed notable activity against both the HeLa and MCF-7 cell lines. Out of the two different cell lines studied, the proliferation of the MCF-7 cell line was arrested to a larger extent than HeLa cells by the complexes under investigation. Though the above mentioned complexes are active against the cell lines under *in vitro* cytotoxicity experiments and show slightly less cytotoxic activity than cisplatin, the cytotoxicity of the complexes (**1–2**) is much better than similar ruthenium complexes containing hydrazone ligands.[53–55] The IC_{50} value of the complexes against NIH-3T3 (non-cancerous cells) is found to be above 240 μM and did not show any damage to normal cells. The experimental results of the cell viability tests suggest that the ruthenium(II) complexes have the ability to arrest the proliferation of cancer cells without causing any damage to the normal cells.

The selectivity index (SI) for each compound is expressed as the IC_{50} of the pure compound in a normal cell line/the IC_{50} of the pure compound in a cancer cell line. The calculated selectivity index for complex **1** and **2** is 5.40, 5.65, 4.11 and 4.35 against HeLa and MCF-7 cell lines, respectively. In the present study, complex **1** demonstrated strong selectivity towards the tested cancer cells.

Apoptotic event: AO–EB and Hoechst staining assays. In order to ascertain the morphological changes the Acridine Orange and Ethidium Bromide (AO and EB) dual staining technique is commonly used. To investigate the mechanistic aspects of cell death and to determine the changes of nuclear morphology, AO and EB dual staining of the MCF-7 cell line treated with complex **1** (50 μM) was carried out and the results are shown in Fig. 8.

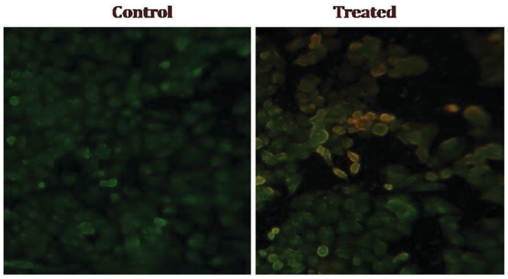

Fig. 8 AO and EB dual staining of MCF-7 cells with the control and treated with complex **1** (50 μM) showing the changes in nuclear morphology.

The experiment was based on the discrimination of live cells from dead cells on the support of morphological changes. Acridine orange passes through the plasma membrane and stains the DNA of live cells with the appearance of green fluorescence. On the other hand, EB is excluded from the cells having an intact plasma membrane and stains the DNA of dead cells, showing orange fluorescence. After treatment of the MCF-7 cells with complex **1** for 24 h and irradiation with visible light significant gross cytological changes of reddish-orange emission are observed with the help of a confocal microscope. The controls, which were incubated in the dark, showed only predominant green emission. These morphological changes indicated that the cells were committed to cell death, mostly *via* an apoptosis pathway.

Additionally, when complex **1** treated MCF-7 cells were stained with Hoechst 33258, apoptotic features such as nuclear shrinkage and chromatin condensation were also observed (Fig. 9). Hence the results of AO–EB and Hoechst staining assays suggest that complex **1** induces apoptosis in MCF-7 cells.

Flow cytometry analysis. In our present inspection, apoptosis was detected by a flow cytometric technique using the Annexin V protocol, with the aid of an Annexin V-FITC apoptosis detection Kit to perform double-staining with propidium iodide and Annexin V-FITC. Hence, we have measured in the various cell populations staining with fluorescein isothiocyanate (FITC labelled Annexin V (green fluorescence) and dye exclusion of the non-vital dye propidium iodide (PI) (red fluorescence negative). The test is easy to perform and discriminates between intact cells ($FITC/PI^-$), and apoptotic ($FITC^+/PI^-$) and necrotic cells ($FITC^+/PI^+$).

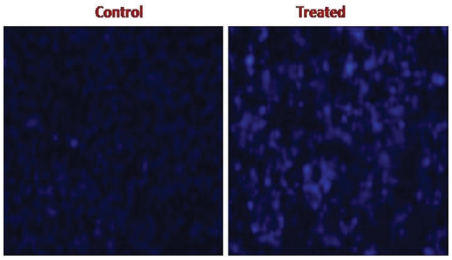

Fig. 9 Hoechst 33258 staining of MCF-7 cells with the control and treated with complex **1** (50 μM) showing the changes in nuclear morphology.

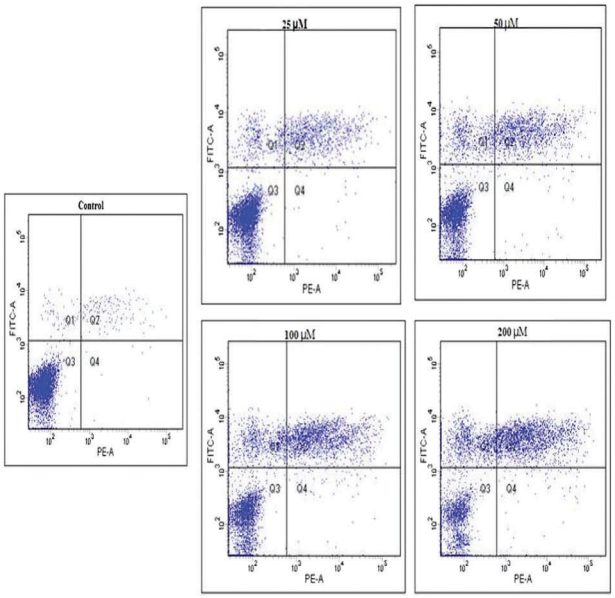

Fig. 10 Flow cytometric results after the exposure of MCF-7 cells to complex **1** at (25–200 μM) for 48 h respectively. Propidium iodide and annexin positive (Q2) and propidium iodide positive (Q4).

The MCF-7 cells were treated with various concentrations (25–200 μM) of complex **1** with a 48 h incubation period. The flow cytometry results are shown in Fig. 10.

The Annexin V^+/PI^+ (Q2) population represented cells undergoing apoptosis and increased by 16.6%, 24.7%, 33.4% and 42.6% for 25 μM, 50 μM, 100 μM and 200 μM concentrations of the investigated ruthenium complex. This observation is in good agreement with the results of fluorescence double staining methods. From these results, we can infer the apoptosis-inducing potential of the complex with different potencies, in accordance with their *in vitro* cytotoxicities.

Conclusions

In this work, two structurally different new organometallic ruthenium complexes $[Ru(CO)(Cl)(PPh_3)_2(O\text{^}S)]$ (**1**) and $[Ru(CO)(PPh_3)_2(N\text{^}O\text{^}S)]$ (**2**) were isolated from the reaction of a (2-hydroxy-5-nitrophenyl)(pyrrolidin-1-yl) methanethione ligand (**L**) with $[RuHCl(CO)(PPh_3)_3]$ under varying experimental conditions. The stoichiometric reaction afforded two ruthenium complexes having distinct ligation, which were characterized using various analytical, spectral and single crystal X-ray crystallographic techniques. It is very interesting to note that one of the obtained complexes, **1**, has the ligand coordinated in the OS coordination mode governed by amide C–N bond cleavage, whereas in complex **2**, the same ligand coordinated in NOS dibasic tridentate fashion. The starting Ru–H precursor can attack the thioamide as a reducing agent during the reaction under reflux conditions *via* amide C–N bond cleavage. The two ruthenium complexes are emissive and possess a light emitting property. Using X-ray structural analysis, supported by a detailed Hirshfeld surface analysis, intermolecular contacts have been analysed and visualized showing that hydrogen bonding is the dominating interaction for the construction of this architecture. *In vitro* cytotoxicity results showed that the two ruthenium complexes exhibit significant anticancer activity against HeLa and MCF-7 cell lines without affecting the normal NIH-3T3 cells. Furthermore, the mode of cell death assessed by AO-EB, Hoechst 33258 staining techniques and flow cytometry analyses revealed that the complexes induce apoptosis in the cancer cell lines. On the basis of these results, the ruthenium complexes may be suitable candidates for further evaluation in *in vivo* experiments.

Experimental section

Materials and instrumentation

All reagents and solvents were of high purity grade and were purchased from commercial sources and used as received. Commercial $RuCl_3{\cdot}3H_2O$ was purchased from Loba-Chemie Pvt. Ltd. The solvents were purified and dried according to standard procedures.[56] The starting material $[RuH(Cl)(CO)(PPh_3)_3]$ was prepared according to a reported method.[57] 5-Nitro salicylaldehyde, pyrrolidine and sulphur were obtained from Aldrich. Microanalytical (C, H, N) data were obtained with a Perkin-Elmer model 240C elemental analyser. Melting points were recorded in the Boetius micro heating table and were uncorrected. The infrared spectra of the complexes were recorded in KBr pellets with a Nicolet iS5 spectrophotometer in the range 4000–400 cm^{-1}. (^1H, ^{13}C) NMR spectra were recorded with a Bruker 400 MHz using $CDCl_3$ as a solvent and tetramethylsilane as an internal reference. The ^{31}P NMR spectra were measured with a Bruker instrument by using $CDCl_3$ as a solvent and *o*-phosphoric acid as an external standard. The mass spectra of the complexes **1** and **2** were recorded using a Q-TOF mass spectrometer. Electronic spectra were recorded on a Varian Cary 300 Bio UV-vis spectrophotometer using cuvettes of 1 cm path length. Emission spectral intensity measurements were carried out by using a Jasco FP-6500 spectrofluorimeter. Thermal analysis measurements were made in the temperature range of 20–900 °C, in an inert atmosphere, at a scanning rate of 10 °C min^{-1} using a Perkin Elmer Pyris 1 thermogravimetric Analyser. 3-(4, 5-Dimethylthiazol-2-yl)-2,5-diphenyltetrazolium bromide (MTT) was purchased from Sigma-Aldrich and used as received. HeLa and MCF-7 cells were received from National centre for cell Science (NCCS), Pune, India. The Annexin V-FITC Kit (APOAF-20TST) from Sigma Aldrich was utilized as per the instructions from the manufacturer. All other chemicals and reagents used for the biological studies were of high quality and biological grade.

Preparation of the (2-hydroxy-5-nitrophenyl)(pyrrolidin-1-yl) methanethione ligand

Ligands of this class were prepared by a modified literature procedure.[58] A mixture of sulphur (0.5 g, 1 mmol), pyrrolidine (1.109 g, 1 mmol), 5-nitrosalicylaldehyde (1.25 g, 0.66 mmol), and acetic acid (0.3 mL) in 20 cm^3 of *N*,*N*-dimethylformamide (DMF) was heated to 100 °C over 1 h with stirring. The mixture

was stirred for an additional 3 h at this temperature and cooled to room temperature. The resulting mixture was poured with stirring into 300 cm^3 of water cooled in an ice bath and the stirring was continued until the oily product had solidified. The solids were filtered, washed with water, dried in air, and dissolved in 600 cm^3 of hot methanol. The remaining solids (mainly unreacted sulphur) were removed by filtration and the red solution was treated with charcoal. The filtered solution was evaporated to 30 cm^3 under reduced pressure to give a faint yellow precipitate, which was recrystallized from warm diethyl ether. Yield = 72%.

Analytical and spectral data for the ligand

(2-Hydroxy-5-nitrophenyl)(pyrrolidin-1-yl)methanethione (L). Color: Pale yellow; yield 72%, M.P.: 148 °C. Anal. calc. for $C_{11}H_{12}N_2O_3S$ (252.29): C, 52.36, H, 4.79, N, 11.10, S, 12.70)%; found C, 52.29, H, 4.69, N, 11.08, S, 12.72)%. Selected IR bands (KBr, ν in cm^{-1}) = 3172 (–OH), 765 (C═S). UV-vis (λ_{max}/nm) 240, 292, 371. ^{1}H NMR (400 MHz, $CDCl_3$): 9.8 (br, 1H, OH), 7.1–8.1 (3H, Ar-H), 3.7–4.0 (4H, α-CH_2), 2.0–2.2 (4H, β-CH_2) ppm. ^{13}C NMR (100 MHz, $CDCl_3$): 189.5 (C═S), 160.6 (C–OH), 139.8, 126.5, 125.7, 122.1, 119.2 (Ar-C), 55, 53.9 (α-CH_2), 26.5, 24.34 (β-CH_2) ppm.

Synthesis of the ruthenium(II) complexes

All the reactions were carried out under anhydrous conditions and the ruthenium complexes were prepared by the following general procedure: To a benzene solution of $[RuHCl(CO)(PPh_3)_3]$ was added the appropriate (2-hydroxy-5-nitrophenyl)(pyrrolidin-1-yl) methanethione ligand. The resulting mixture was kept at room temperature and under reflux conditions for 5 h. Coordination was immediate, as a change of colour from yellow into red was observed. The reaction mixture changed colour gradually and the reactions were monitored by TLC. The solution was concentrated to about 3 mL and petroleum ether (60–80 °C) was added. The obtained solid residue was filtered and washed with hexane. On evaporation of the resulting solution, pure compounds were obtained and were dried under vacuum to give reasonable yields (72–80%).

$[Ru(CO)(Cl)(PPh_3)_2(O\hat{}S)]$(1). Color: Red. Yield: 72%. M.P.: 202 °C. Anal. calc. For $C_{44}H_{34}ClNO_4P_2RuS$ (871.28 g mol^{-1}): C, 60.65; H, 3.93; N, 1.60; S, 3.68%. Found: C, 60.25; H, 3.66; N, 1.50; S, 3.58%. FT-IR (KBr, cm^{-1}) 1316 (C–O), 744 (C═S), 1954 (Ru–CO). UV-vis $CHCl_3$, λ_{max}/nm; ε/dm^3 mol^{-1} cm^{-1}: 555 (936), 395 (3159), 270 (7642), 242 (10 524). ^{1}H-NMR (400 MHz, $CDCl_3$): 8.0 (s, 1H, HC═S), 7.1–7.6 (m, 33H, aromatic) ppm. ^{13}C NMR (100 MHz, $CDCl_3$): 126.2, 127.6, 128.1, 128.5, 128.6, 129.6, 130.2, 130.8, 131, 131.2, 131.6, 131.9, 132.1, 132.3, 132.9, 134.4, 134.5, 134.7, 134.8, 137.4 (Ar-C_{PPh3} + Ar-C_{Ligand}), 170.2 (C═S), 186.9 (C═O) ppm. ^{31}P NMR (162 MHz, $CDCl_3$) 27.26 ppm (s, PPh_3). ESI-MS: calculated for $C_{44}H_{34}ClNO_4P_2RuS$ is 871.2; found 871.0.

$[Ru(CO)(PPh_3)_2(N\hat{}O\hat{}S)]$(2). Color: Red. Yield: 80%. M.P.: 165 °C. Anal. calc. For $C_{48}H_{42}N_2O_4P_2RuS$ (905.90 g mol^{-1}): C, 63.63; H, 4.67; N, 3.09; S, 3.53%. Found: C, 63.25; H, 4.36; N, 3.15; S, 3.45%. FT-IR (KBr, cm^{-1}) 1315 (C–O), 695 (C–S), 1953 (Ru–CO), 518 (Ru–N). UV-vis $CHCl_3$, λ_{max}/nm; ε/dm^3 mol^{-1} cm^{-1}: 560 (906), 392 (3022), 271 (7312), 241 (10 143). ^{1}H-NMR (400 MHz, $CDCl_3$): 7.1–7.6 (m, 33H, aromatic), 2.8–2.9 (s, 4H), 3.3–3.7 (s, 3H) ppm. ^{13}C NMR (100 MHz, $CDCl_3$): 24.5, 26.4, 29.6, 45.5, 53.4 (−CH_2 and –CH), 117.7, 123.6, 125.9, 127.6, 127.7, 128.1, 128.5, 128.6, 128.7, 128.8, 130.3, 131.6, 132, 132.1, 132.2, 132.3, 132.4, 133.8, 133.9, 134.5, 140.1 (Ar-C_{PPh3} + Ar-C_{Ligand}), 158.8 (C–S), 190.6 (C═O) ppm. ^{31}P NMR (162 MHz, $CDCl_3$) 43.32 (s, PPh_3). ESI-MS: calculated for $C_{48}H_{42}N_2O_4P_2RuS$ is 905.9; found 905.2.

X-ray crystallography

Single crystals of the ligand **L** and complexes **1** and **2** suitable for X-ray diffraction studies were grown by slow evaporation of methanol and a dichloromethane–acetonitrile mixture at room temperature. A single crystal of suitable size was mounted in turn on an Gemini A Ultra Oxford Diffraction automatic diffractometer equipped with a CCD detector, and used for data collection. X-ray intensity data were collected with graphite monochromated Mo Kα radiation (λ = 0.71073 Å) at a temperature of 295(2) K, with the ω scan mode. Ewald sphere reflections were collected up to $2\theta = 50.10^\circ$. Lorentz, polarization and empirical absorption corrections using spherical harmonics implemented in the SCALE3, ABSPACK scaling algorithm[59] were applied. The structures were solved by the direct method. All the non-hydrogen atoms were refined anisotropically using the full-matrix, least-squares technique on F^2. The Olex2,[60] SHELXS, and SHELXL[61] programs were used for all the calculations. Atomic scattering factors were those incorporated in the computer programs.

Theoretical calculations

The calculations were carried out using the Gaussian09 program.[62] The DFT/B3LYP[63,64] method was used for the geometry optimization and electronic structure determination. The calculations were performed using the 6-31G** functions for carbon, nitrogen, sulfur, chloride, oxygen and phosphorus atoms and 6-31G for hydrogen. The DZVP basis set[65] with *f* functions with exponents 1.94722036 and 0.748930908 was used to describe the ruthenium atom. The 6-31G** and 6-31G basis sets were taken from the Gaussian09 program. The PCM solvent model was used in the Gaussian calculations with dichloromethane as the solvent. Frequency calculation was carried out, verifying whether the optimized molecular structure corresponds to energy minimum, thus only positive frequencies were expected. The CIS(D) (single excitation configuration interaction with doubles correction) method was used to describe the first singlet and triplet excited states of the ruthenium complex.[66] The contribution of a group to a molecular orbital was calculated using Mülliken population analysis. GaussSum 3.0[67] was used to calculate group contributions to the molecular orbitals and prepare the partial density of states (DOS) and overlap partial density of states (OPDOS) diagram. These spectra were created by convoluting the molecular orbital information with GAUSSIAN curves of unit height and FWHM of 0.3 eV. The electrostatic potential (ESP) surfaces were plotted by using gOpenMol v2.31 program. The Hirshfeld surfaces analysis were performed using the crystal geometries

that were used as input to the TONTO[68] integrated with the Crystal explorer program.[69]

Cytotoxicity: maintenance of cell lines

The tests were done in monolayer cells detached with trypsin-ethylenediaminetetraacetic acid (EDTA) to make single cell suspensions and viable cells were counted using a hemocytometer and diluted with medium containing 5% FBS to give a final density of 1×10^5 cells per mL. One hundred microlitres per well of cell suspension were seeded into 96-well plates at a plating density of 10 000 cell per well and incubated to allow for cell attachment at 37 °C, under conditions of 5% CO_2, 95% air and 100% relative humidity. After 24 h, the cells were treated with serial concentrations of the test complexes. The complexes were initially dissolved in neat DMSO and an aliquot sample solution was diluted to twice the desired final maximum test concentration with a serum free medium. An additional four serial dilutions were made to provide a total of five sample concentrations. Aliquots of 100 μL of these different sample dilutions were added to the appropriate wells already containing 100 μL of medium, resulting in the required final sample concentrations. Following sample addition, the plates were incubated for an additional 48 h at 37 °C, 5% CO_2, 95% air and 100% relative humidity. The medium without complexes served as a control and triplicates were maintained for all concentrations.

MTT assay

3-[4,5-Dimethylthiazol-2-yl]2,5-diphenyltetrazolium bromide (MTT) is a yellow water soluble tetrazolium salt. A mitochondrial enzyme in living cells, succinate-dehydrogenase, cleaves the tetrazolium ring, converting the MTT to insoluble purple formazan. Therefore, the amount of formazan produced is directly proportional to the number of viable cells. After 48 h of incubation, 15 μL of MTT (5 mg mL^{-1}) in phosphate buffered saline (PBS) was added to each well and incubated at 37 °C for 4 h. The medium with MTT was then flicked off and the formed formazan crystals were solubilized in 100 μL of DMSO and then the absorbance was measured at 570 nm using a micro plate reader. The % cell inhibition was determined using the following formula.

$$\%\ \text{Cell Inhibition} = 100 - \text{Abs (sample)/Abs (control)} \times 100.$$

A nonlinear regression graph was plotted between % cell inhibition and Log concentration and IC_{50} was determined using GraphPad Prism software.

Partition coefficient determination

The hydrophobicity values of complexes **1** and **2** were measured by using the ''Shake flask'' method in octanol–water phase partitions as reported earlier.[70] The complexes were dissolved in a mixture of water and *n*-octanol followed by shaking for 1 hour. The mixture was allowed to settle over a period of 30 minutes and the resulting two phases were collected separately without cross contamination of one solvent layer into another. The concentration of the complexes in each phase was determined by UV-vis absorption spectroscopy at room temperature. The results are given as the mean values obtained from three independent experiments.

Fluorescent double staining experiment

Acridine Orange and Ethidium Bromide (AO and EB) staining was performed as follows: The MCF-7 cells were treated with complex **1** at 50 μM and incubated for 24 hours in a CO_2 incubator at 37 °C. The cells were removed by trypsination and collected by centrifugation including the non adherent cells. The cell pellet was re-suspended in medium and the cell suspensions (25 μL) were transferred to glass slides. Dual fluorescent staining solution (1 μL) containing 100 μg mL^{-1} AO and 100 μg mL^{-1} EB (AO/EB, Sigma) was added to each suspension and then covered with a coverslip. The morphology of apoptotic cells was examined and the cells were counted within 20 min using a fluorescence microscope.

Hoechst 33258 staining method

Hoechst 33258 staining was done using a method described earlier but with slight modifications. 5×10^5 MCF-7 cells were treated with IC_{50} concentrations of complex **1** for 24 h in a 6-well culture plate and fixed with 4% paraformaldehyde followed by permeabilization with 0.1% Triton X-100. The cells were then stained with 50 μg mL^{-1} Hoechst 33258 for 30 min at room temperature. The cells undergoing apoptosis, represented by the morphological changes of apoptotic nuclei, were observed and imaged using an epifluorescence microscope (Carl Zeiss, Germany).

Apoptosis detection-flow cytometry analysis

MCF-7 cells were grown in 6-well plates and defined at four different concentrations of complex **1** with a 48 h incubation period. The Annexin V-FITC kit uses annexin V conjugated with fluorescein isothiocyanate (FITC) to label phosphatidylserine sites on the membrane surface of apoptotic cells. Briefly, the cells were trypsinised and washed with Annexin binding buffer and incubated with Annexin V FITC and PI for 30 minutes and immediately analysed using a FACS Aria-II flow cytometer. The forward and side scattering parameters were adjusted to keep the background fluorescence to a minimum. The results were carefully analysed by using DIVA software and the percentage of positive cells was calculated.

Acknowledgements

R. R. K. thanks the DST-INSPIRE Program for the financial assistance as a Senior Research Fellow (IF130075). We thank UGC-SAP and DST-India (FIST programme) for the use of the Bruker 400 MHz NMR UV-visible and Fluorescence spectral facilities at the School of Chemistry, Bharathidasan University. The GAUSSIAN09 calculations have been carried out using resources provided by the Wroclaw Centre for Networking and Supercomputing, WCSS, Wroclaw, Poland (http://wcss.pl), Grant Number 18.

References

1 L. J. Goossen, M. Blanchot, K. S. M. Salih, R. Karch and A. Rivas-Nass, *Org. Lett.*, 2008, **10**, 4497–4499.
2 M. Iwata, R. Yazaki, I. H. Chen, D. Sureshkumar, N. Kumagai and M. Shibasaki, *J. Am. Chem. Soc.*, 2011, **133**, 5554–5560.
3 D. L. Klayman, J. P. Scovill, J. F. Bartosevich and J. Bruce, *J. Med. Chem.*, 1983, **26**, 35–39.
4 C. Shipman, S. H. Smith, J. C. Drach and D. L. Klayman, *Antiviral Res.*, 1986, **6**, 197–222.
5 D. L. Klayman, J. P. Scovill, J. F. Bartosevich and C. J. Mason, *J. Med. Chem.*, 1979, **22**, 1367–1373.
6 S. Miranda, E. Vergara, F. Mohr, D. de Vos, E. Cerrada, A. Mendía and M. Laguna, *Inorg. Chem.*, 2008, **47**, 5641–5648.
7 R. Raj Kumar, M. K. Mohamed Subarkhan and R. Ramesh, *RSC Adv.*, 2015, **5**, 46760–46773.
8 R. A. Begum, D. Powell and K. Bowman-James, *Inorg. Chem.*, 2006, **45**, 964–966.
9 T.-a. Koizumi, T. Teratani and K. Okamoto, *Inorg. Chim. Acta*, 2010, **363**, 2474.
10 S. Kagaya, H. Miyazaki, M. Ito, K. Tohda and T. Kanbara, *J. Hazard. Mater.*, 2010, **175**, 1113–1115.
11 A. Kanchanadevi, R. Ramesh and D. Semeril, *J. Organomet. Chem.*, 2016, **808**, 68–77.
12 V. A. Kozlov, D. V. Aleksanyan, Y. V. Nelyubina, K. A. Lyssenko, E. I. Gutsul, L. N. Puntus, A. A. Vasil'ev, P. V. Petrovskii and I. L. Odinets, *Organometallics*, 2008, **27**, 4062–4070.
13 S. K. Hadjikakou, I. I. Ozturk, M. N. Xanthopoulou, P. C. Zachariadis, S. Zartilas, S. Karkabounas and N. Hadjiliadis, *J. Inorg. Biochem.*, 2008, **102**, 1007–1015.
14 T. Cupido, J. Tulla-Puche, J. Spengler and F. Albericio, *Curr. Opin. Drug Discovery Dev.*, 2007, **10**, 768–783.
15 H. E. Bryndza and W. Tam, *Chem. Rev.*, 1988, **88**, 1163–1188.
16 L. Dong, S. B. Duckett, K. F. Ohman and W. D. Jones, *J. Am. Chem. Soc.*, 1992, **114**, 151–160.
17 E. Furimsky, *Catal. Rev.*, 1983, **25**, 421–458.
18 Y. T. Shah and D. C. Cronauer, *Catal. Rev.*, 1979, **20**, 209–301.
19 R. J. Kinney, W. D. Jones and R. G. Bergman, *J. Am. Chem. Soc.*, 1978, **100**, 7902–7915.
20 C. N. Satterfield, C. M. Smith and M. Ingalls, *Ind. Eng. Chem. Process Des. Dev.*, 1985, **24**, 1000–1004.
21 F. A. Cotton, L. M. Daniels, C. A. Murillo and X. Wang, *Inorg. Chem.*, 1997, **36**, 896–901.
22 K. Takano, A. Inagaki and M. Akita, *Chem. Lett.*, 2006, **35**, 434–435.
23 S. Caddick, F. G. N. Cloke, P. B. Hitchcock and A. K. de K. Lewis, *Angew. Chem.*, 2004, **116**, 5948–5951.
24 O. V. Ozerov, C. Guo, V. A. Papkov and B. M. Foxman, *J. Am. Chem. Soc.*, 2004, **126**, 4792–4793.
25 S. Burling, M. F. Mahon, R. E. Powell, M. K. Whittlesey and J. M. J. Williams, *J. Am. Chem. Soc.*, 2006, **128**, 13702–13703.
26 A. L. Balch, Y. W. Chan, M. M. Olmstead, M. W. Renner and F. E. Wood, *J. Am. Chem. Soc.*, 1988, **110**, 3897–3902.
27 W.-L. Man, J. Xie, Y. Pan, W. W. Y. Lam, H.-K. Kwong, K.-W. Ip, S.-M. Yiu, K.-C. Lau and T.-C. Lau, *J. Am. Chem. Soc.*, 2013, **135**, 5533–5536.
28 M. Tayebani, K. Feghali, S. Gambarotta and C. Bensimon, *Organometallics*, 1997, **16**, 5084–5088.
29 Y. Lei, A. D. Wrobleski, J. E. Golden, D. R. Powell and J. Aubé, *J. Am. Chem. Soc.*, 2005, **127**, 4552–4553.
30 J. B. Bonanno, T. P. Henry, D. R. Neithamer, P. T. Wolczanski and E. B. Lobkovsky, *J. Am. Chem. Soc.*, 1996, **118**, 5132–5133.
31 T. Koreeda, T. Kochi and F. Kakiuchi, *J. Am. Chem. Soc.*, 2009, **131**, 7238–7239.
32 P. Vijayan, P. Viswanathamurthi, P. Sugumar, M. N. Ponnuswamy, J. G. Malecki, K. Velmurugan, R. Nandhakumar, M. D. Balakumaran and P. T. Kalaichelvan, *Appl. Organomet. Chem.*, 2017, **31**, 1–23.
33 E. R. Jamieson and S. J. Lippard, *Chem. Rev.*, 1999, **99**, 2467–2498.
34 I. Kostova, *Curr. Med. Chem.*, 2006, **13**, 1085–1107.
35 G. Zhao and H. Lin, *Curr. Med. Chem.: Anti-Cancer Agents*, 2005, **5**, 137–147.
36 G. Sathyaraj, T. Weyhermüller and B. U. Nair, *Eur. J. Med. Chem.*, 2010, **45**, 284–291.
37 S. K. Mandal and A. R. Chakravarty, *J. Chem. Soc., Dalton Trans.*, 1992, 1627–1633, DOI: 10.1039/dt9920001627.
38 C. Jayabalakrishnan and K. Natarajan, *Transition Met. Chem.*, 2002, **27**, 75–79.
39 M. Cao, L. V. Do, N. W. Hoffman, M.-L. Kwan, J. K. Little, J. M. McGilvray, C. B. Morris, B. C. Söderberg, A. Wierzbicki and T. R. Cundari, *Organometallics*, 2001, **20**, 2270–2279.
40 S. Goswami, A. Chakravarty and A. Chakravorty, *Inorg. Chem.*, 1982, **21**, 2737–2742.
41 K. Chichak, U. Jacquemard and Neil R. Branda, *Eur. J. Inorg. Chem.*, 2002, 357–368.
42 K. Natarajan, R. K. Poddar and U. Agarwala, *J. Inorg. Nucl. Chem.*, 1977, **39**, 431–435.
43 S. Watkins and F. Fronczek, *Acta Crystallogr., Sect. B: Struct. Sci.*, 1982, **38**, 270–271.
44 F. B. McCormick, D. D. Cox and W. B. Gleason, *Organometallics*, 1993, **12**, 610–612.
45 F. Basuli, S.-M. Peng and S. Bhattacharya, *Inorg. Chem.*, 2001, **40**, 1126–1133.
46 N. Chitrapriya, V. Mahalingam, L. C. Channels, M. Zeller, F. R. Fronczek and K. Natarajan, *Inorg. Chim. Acta*, 2008, **361**, 2841–2850.
47 R. Raveendran and S. Pal, *Polyhedron*, 2008, **27**, 655–662.
48 H. H. Nguyen, N. Hoang and U. Abram, *Transition Met. Chem.*, 2010, **35**, 89–93.
49 I. N. Booysen, A. Adebisi, M. P. Akerman, O. Q. Munro and B. Xulu, *J. Coord. Chem.*, 2016, **69**, 1641–1652.
50 J. G. Małecki, *Polyhedron*, 2010, **29**, 1973–1979.
51 S. Wolff, D. Grimwood, J. McKinnon, M. Turner, D. Jayatilaka and M. Spackman, there is no corresponding record for this reference.
52 B. K. Panda, K. Ghosh, S. Chattopadhyay and A. Chakravorty, *J. Organomet. Chem.*, 2003, **674**, 107–115.

53 M. Mohanraj, G. Ayyannan, G. Raja and C. Jayabalakrishnan, *J. Photochem. Photobiol., B*, 2016, **158**, 164–173.
54 P. Sathyadevi, P. Krishnamoorthy, N. S. P. Bhuvanesh, P. Kalaiselvi, V. Vijaya Padma and N. Dharmaraj, *Eur. J. Med. Chem.*, 2012, **55**, 420–431.
55 M. Mohanraj, G. Ayyannan, G. Raja and C. Jayabalakrishnan, *Mater. Sci. Eng., Proc. Conf.*, 2016, **69**, 1297–1306.
56 B. S. Furniss, *Vogel's textbook of practical organic chemistry*, Pearson Education India, 1989.
57 N. Ahmad, J. J. Levison, S. Robinson, M. Uttley, E. Wonchoba and G. Parshall, *Inorg. Synth.*, 2007, **15**, 45–64.
58 Y. Nojima, M. Nonoyama and K. Nakajima, *Polyhedron*, 1996, **15**, 3795–3809.
59 CrysAlis RED, Oxford Diffraction Ltd., Version 1.171.37.35g.
60 R. J. Gildea, L. J. Bourhis, O. V. Dolomanov, R. W. Grosse-Kunstleve, H. Puschmann, P. D. Adams and J. A. K. Howard, *J. Appl. Crystallogr.*, 2011, **44**, 1259–1263.
61 G. Sheldrick, *Acta Crystallogr., Sect. A: Found. Crystallogr.*, 2008, **64**, 112–122.
62 M. Frisch, G. Trucks, H. Schlegel, G. Scuseria, M. Robb, J. Cheeseman, G. Scalmani, V. Barone, B. Mennucci and G. Petersson, *Gaussian Inc.*, Wallingford CT, 2009139.
63 A. D. Becke, *J. Chem. Phys.*, 1993, **98**, 5648–5652.
64 C. Lee, W. Yang and R. G. Parr, *Phys. Rev. B: Condens. Matter Mater. Phys.*, 1988, **37**, 785–789.
65 K. Eichkorn, F. Weigend, O. Treutler and R. Ahlrichs, *Theor. Chem. Acc.*, 1997, **97**, 119–124.
66 M. Head-Gordon, R. J. Rico, M. Oumi and T. J. Lee, *Chem. Phys. Lett.*, 1994, **219**, 21–29.
67 A. Boyle, *J. Comput. Chem.*, 2008, **29**, 839.
68 D. Jayatilaka, D. Grimwood, A. Lee, A. Lemay, A. Russel, C. Taylo and S. Wolff, *Whitton, TONTO—A System for Computational Chemistry*, 2005.
69 I. Soussi, A. Maalaoui, O. Pérez, M. Rzaigui and S. Akriche, *J. Cluster Sci.*, 2016, **27**, 1863–1876.
70 R. K. Gupta, R. Pandey, G. Sharma, R. Prasad, B. Koch, S. Srikrishna, P.-Z. Li, Q. Xu and D. S. Pandey, *Inorg. Chem.*, 2013, **52**, 3687–3698.

